



Effects of orbital
acceleration on
interglacial climates

V. Varma et al.

Transient simulations of the present and the last interglacial climate using a coupled general circulation model: effects of orbital acceleration

V. Varma^{1,a}, M. Prange^{1,2}, and M. Schulz^{1,2}

¹MARUM – Center for Marine Environmental Sciences, University of Bremen, Bremen, Germany

²Faculty of Geosciences, University of Bremen, Bremen, Germany

^anow at: Department of Meteorology, Stockholm University, Stockholm, Sweden

Received: 28 June 2015 – Accepted: 2 July 2015 – Published: 21 July 2015

Correspondence to: V. Varma (vidya.varma@misu.su.se)

Published by Copernicus Publications on behalf of the European Geosciences Union.

Title Page

Abstract

Introduction

Conclusions

References

Tables

Figures



Back

Close

Full Screen / Esc

Printer-friendly Version

Interactive Discussion



Abstract

Numerical simulations provide a considerable aid in studying past climates. Out of the various approaches taken in designing numerical climate experiments, transient simulations have been found to be the most optimal when it comes to comparison with proxy data. However, multi-millennial or longer simulations using fully coupled general circulation models are computationally very expensive such that acceleration techniques are frequently applied. In this study, we compare the results from transient simulations of the present and the last interglacial with and without acceleration of the orbital forcing, using the comprehensive coupled climate model CCSM3 (Community Climate System Model 3). Our study shows that in most parts of the world, the simulation of long-term variations in interglacial surface climate is not significantly affected by the use of the acceleration technique (with an acceleration factor 10) and, hence, large-scale model-data comparison of surface variables is not hampered. However, in high-latitude regions where the surface climate has a direct connection to the deep ocean, e.g. in the Southern Ocean or the Nordic Seas, acceleration-induced biases in sea-surface temperature evolution may occur with potential influence on the dynamics of the overlying atmosphere.

1 Introduction

Earth's past climate is simulated numerically through either equilibrium simulations ("time slice experiments") or through transient simulations with time-dependent boundary conditions using climate models. In equilibrium simulations, the boundary conditions are not varied temporally but rather kept fixed under the assumption that the Earth system is in equilibrium with them (e.g. Braconnot et al., 2007; Lunt et al., 2013; Milker et al., 2013). Evidently, only limited information regarding the temporal evolution of the dynamic system is obtained by the time slice approach. This approach signifi-

GMDD

8, 5619–5641, 2015

Effects of orbital acceleration on interglacial climates

V. Varma et al.

Title Page

Abstract

Introduction

Conclusions

References

Tables

Figures



Back

Close

Full Screen / Esc

Printer-friendly Version

Interactive Discussion



tion for the application of this acceleration technique is that orbital forcing operates on much longer timescales than those inherent in the atmosphere and upper ocean layers (Lorenz and Lohmann, 2004).

2 Methods

5 Multi-millennial transient simulations were performed using the comprehensive global CGCM CCSM3 (Community Climate System Model version 3). NCAR's (National Center for Atmospheric Research) CCSM3 is a state-of-the-art fully coupled model, composed of four separate components representing atmosphere, ocean, land and sea ice (Collins et al., 2006). Here, we employ the low-resolution version described in detail
10 by Yeager et al. (2006). In this version the resolution of the atmospheric component is given by T31 (3.75° transform grid), with 26 layers in the vertical, while the ocean has a nominal resolution of 3° with refined meridional resolution (0.9°) around the equator and a vertical resolution of 25 levels. The sea-ice component shares the same horizontal grid with the ocean model.

15 The time periods of interest in this study are the present interglacial (PIG) (11.7–0 kyr BP, kiloyears before present) and the last interglacial (LIG) (ca. 130–115 kyr BP). On these multi-millennial time-scales, it is the periodic changes in the Earth's orbital parameters that cause the modifications of seasonal and latitudinal distribution of insolation at the top of the atmosphere (Berger, 1978), acting as the prime forcing of
20 long-term interglacial climate change.

The climatic precession parameter increased during both the PIG and the LIG (from ~ 127 kyr BP onward; Fig. 1). As a result, there was a weakening of the seasonal insolation amplitude in the Northern Hemisphere resulting in a decrease in the boreal summer insolation (Berger, 1978). For the LIG, the variability in climatic precession
25 was more pronounced compared to the PIG due to a larger orbital eccentricity. Hence, the effect of orbital forcing on climate is expected to be stronger (Fig. 1b). Additionally,

GMDD

8, 5619–5641, 2015

Effects of orbital acceleration on interglacial climates

V. Varma et al.

Title Page

Abstract

Introduction

Conclusions

References

Tables

Figures

◀

▶

◀

▶

Back

Close

Full Screen / Esc

Printer-friendly Version

Interactive Discussion



the obliquity decreased by ~ 0.5 to 1° over the interglacials resulting in a decrease of insolation in the summer hemisphere.

Accelerated and non-accelerated transient simulations covering the two interglacials (9 to 2 kyr BP for the PIG and 130 to 120 kyr BP for the LIG) were carried out under varying orbital forcing only. The experimental set-ups for the accelerated PIG and LIG simulations are described in Varma et al. (2012) and Bakker et al. (2013), respectively. In both simulations, the orbital forcing is accelerated by a factor 10. Therefore, climate trends over 7000 (PIG experiment) and 10 000 years (LIG experiment) imposed by the external orbitally driven insolation changes, are represented in the accelerated experiments by only 700 and 1000 simulation years, respectively. In the present study, an ensemble mean of three transient runs, starting from slightly different initial conditions, is used for the accelerated PIG (for details see Varma et al., 2012). We note that the conclusions of this study are valid for each individual accelerated transient simulation and hence are unaffected by the ensemble averaging. Single transient simulations represent all other scenarios (i.e. non-accelerated PIG, accelerated and non-accelerated LIG). Throughout both interglacial runs pre-industrial aerosol and ozone distributions as well as modern ice sheet configurations were prescribed. The greenhouse gas concentrations in the LIG runs take the mean value for the period 130–120 kyr BP (i.e. $\text{CO}_2 = 272$ ppm, $\text{CH}_4 = 622$ ppb and $\text{N}_2\text{O} = 259$ ppb; Louergue et al., 2008; Lüthi et al., 2008; Spahni et al., 2005). Throughout the PIG experiments, greenhouse gas concentrations were kept constant at pre-industrial values ($\text{CO}_2 = 280$ ppm, $\text{CH}_4 = 760$ ppb and $\text{N}_2\text{O} = 270$ ppb).

The non-accelerated PIG transient simulation was initialized as follows: from a pre-industrial quasi-equilibrium simulation (Merkel et al., 2010), the model was integrated for 400 years with fixed boundary conditions representing 9 kyr BP orbital forcing and pre-industrial atmospheric composition. The transient simulation started from the final state of this time slice run. The LIG transient simulations were initialized as follows: the final state of the 9 kyr BP simulation was used to initialize a 130 kyr BP time slice run. This 130 kyr BP run was integrated for another 400 years with fixed boundary conditions

GMDD

8, 5619–5641, 2015

Effects of orbital acceleration on interglacial climates

V. Varma et al.

Title Page

Abstract

Introduction

Conclusions

References

Tables

Figures



Back

Close

Full Screen / Esc

Printer-friendly Version

Interactive Discussion



representing 130 kyr BP orbital forcing and atmospheric composition as in the transient LIG runs (see above), which were then started from the final 130 kyr BP state.

Forcing of accelerated and non-accelerated transient runs differs only in the rate of change of orbital parameters. This approach allows the identification of acceleration effects by direct comparison of the accelerated and non-accelerated runs. For the analyses of the model results decadal means (referring to model years) have been used from all the transient simulations.

3 Results

Figure 2 shows the simulated evolution of annual-mean global ocean temperatures at depths of 4 m (surface), 437 m and 1884 m for both interglacials. The surface temperature for the PIG shows considerable differences between the accelerated and non-accelerated runs, especially during the early-to-mid PIG (Fig. 2a). While there is a pronounced decreasing trend in surface temperature for the non-accelerated run during the time period 9–7 kyr BP, this is not captured in the accelerated PIG run. The 437 m temperature evolution for the PIG shows reasonably similar trends in both accelerated and non-accelerated simulations (Fig. 2c). However, as we go further deep, at 1884 m there is an overall significant difference quantitatively between the accelerated and non-accelerated PIG runs (Fig. 2e). While there is a drop of $\sim 0.4^\circ\text{C}$ in the deep-ocean temperature in the non-accelerated simulation during the early PIG, the accelerated run is underestimating this decreasing trend and shows a strongly delayed and much more stable response.

For the LIG, the temperatures at the surface and at 437 m depths show overall similar responses in both accelerated and non-accelerated runs, though there are some differences during the late LIG (Fig. 2b and d). However, like in the PIG, the response of 1884 m temperature is quite contrasting in the LIG as well (Fig. 2f). The deep-ocean temperature is showing a decreasing trend during the early-to-mid LIG and then an increasing trend for the mid-to-late LIG in the non-accelerated run (Fig. 2f). Not only

Effects of orbital acceleration on interglacial climates

V. Varma et al.

Title Page

Abstract

Introduction

Conclusions

References

Tables

Figures



Back

Close

Full Screen / Esc

Printer-friendly Version

Interactive Discussion



this trend variability is missing in the accelerated run, but also the general temperature evolution during the LIG is quantitatively underestimated. While the change in 1884 m temperature during the LIG is $\sim 0.3^\circ\text{C}$ in the non-accelerated simulation, it is just about 0.06°C in the accelerated run (Fig. 2f).

Figure 3 represents the evolution of zonally averaged surface temperature for both interglacials. For the PIG, in response to orbital forcing, it is the high latitudes that show a robust cooling response, in both accelerated and non-accelerated simulations (Fig. 3a and b). It also shows a warming of the tropics during the mid-to-late PIG in both the simulations. The anomaly between simulations with and without orbital acceleration (Fig. 3c) clearly shows that there are evident disparities in the high latitudes especially during the early-to-mid PIG, when the southern high-latitude cooling in the accelerated simulation lags the cooling in the non-accelerated run. For the LIG, the northern high latitudes tend to show a slight warming between ~ 130 – 125 kyr BP and then an intense cooling trend afterwards in both non-accelerated and accelerated simulations (Fig. 3d and e). The southern high latitudes show a cooling trend during the early LIG in the non-accelerated run, followed by a warming trend during the late LIG. By contrast, a steady cooling trend in the southern high latitudes is simulated in the accelerated run. The low latitudes show strongest warming from mid-to-late LIG in both the simulations.

Figure 4 displays the evolution of zonally averaged zonal wind at 850 hPa for both interglacials. A pronounced strengthening of the zonal wind circulation in the southern high mid-latitudes (ca. 50 – 60°S) is simulated in the non-accelerated PIG run (Fig. 4a). There is a similar pattern observed in the accelerated simulation as well but less intense and delayed in time compared to its non-accelerated counterpart (Fig. 4b). This wind intensification at the southern flank of the Southern Westerly Wind (SWW) belt is accompanied by a decrease of zonal wind speed at the northern flank of the SWW region (ca. 30 – 40°S), which can be depicted as a general poleward shift of the SWW during the PIG under orbital forcing as described in an earlier study (Varma et al., 2012). Similarly, for the LIG as well a poleward shift of SWW under orbital forcing

Effects of orbital acceleration on interglacial climates

V. Varma et al.

[Title Page](#)[Abstract](#)[Introduction](#)[Conclusions](#)[References](#)[Tables](#)[Figures](#)[Back](#)[Close](#)[Full Screen / Esc](#)[Printer-friendly Version](#)[Interactive Discussion](#)

is observed in both non-accelerated and accelerated simulations, albeit more robust compared to the PIG response (Fig. 4d and e).

Figure 5 shows the evolution of global surface temperature during the PIG, for both non-accelerated and accelerated runs decomposed into Empirical Orthogonal Functions (EOFs). The first EOF shows a general cooling trend of the high latitudes in both hemispheres in both non-accelerated and accelerated simulations. The cooling is more pronounced in the northern high latitudes in response to the changes in insolation. Maximum cooling is observed around Baffin Bay extending up to the Labrador Sea in both the simulations (Fig. 5a and e). Sea-ice effects play a role here in amplifying the climatic response to the orbital forcing. Another feature observed in both simulations is the general warming trend in the tropics, especially over the Sahel and Indian regions, which is mainly attributed to climate feedbacks associated with orbital-induced weakening of the monsoons (e.g. Bakker et al., 2013). The second EOF shows strong variability in the Nordic Seas, associated with shifts in the sea-ice margin in both non-accelerated and accelerated simulations (Fig. 5c and g). However, even though the general spatial patterns of the two leading EOFs are similar between the accelerated and the non-accelerated simulation, some differences in the EOF maps are evident especially in the northern North Atlantic and Nordic Seas as well as in the Southern Ocean. Moreover, the first principal component exhibits a rather linear trend throughout the Holocene in the accelerated simulation (Fig. 5f), whereas an increased rate of change can be observed during the early Holocene in the first principal component of the non-accelerated run (Fig. 5b). We further note that the leading EOF contributes more to the total surface temperature variance in the accelerated simulation (56%) than in the non-accelerated run (29%) since multi-centennial to multi-millennial modes of internal climate variability are not captured in the accelerated simulation and, hence, cannot add to the total temperature variability.

The spatio-temporal evolution of global surface temperature during the LIG is represented in Fig. 6 by means of the two leading EOFs. The observed high latitude cooling in the Northern Hemisphere is more pronounced in the LIG compared to the PIG in

Effects of orbital acceleration on interglacial climates

V. Varma et al.

Title Page

Abstract

Introduction

Conclusions

References

Tables

Figures



Back

Close

Full Screen / Esc

Printer-friendly Version

Interactive Discussion



line with larger insolation changes. Similar is the case with the tropics where the warming is more pronounced compared to the PIG. These patterns are very similar in the first EOFs of both non-accelerated and accelerated simulations (Fig. 6a and e). The second EOFs reflect strong variability in the northern North Atlantic without showing any clear orbital trend indicative of internal climate variability. In general, both non-accelerated and accelerated simulations share similar response patterns in the second EOF (Fig. 6c and g). However, both leading EOFs reveal pronounced differences between non-accelerated and accelerated runs in the Southern Ocean sector, similar to what has been found for the PIG simulations.

Figure 7 shows the leading two EOFs for global precipitation during the PIG for both non-accelerated and accelerated simulations. The first EOF of both simulations reveals a general weakening of the North African and Indian monsoon systems along with a strengthening of Southern Hemisphere monsoons (Fig. 7a and e). The second EOF does not contain a long-term (orbitally driven) trend, but rather shows a pattern of (multi-)decadal tropical precipitation variability. This EOF is not significantly affected by the acceleration either.

Figure 8 depicts the evolution of global precipitation during the LIG in both non-accelerated and accelerated simulations. Similar to the PIG, there is a decreasing trend in North African and Indian monsoonal rainfall along with increasing precipitation over South America, Southern Africa and Australia (Fig. 8a and e), albeit more pronounced than during the PIG. The second EOF contains a long-term (orbitally forced) signal, but explains only ca. 8% of the total variance in both the accelerated and the non-accelerated run. Again, orbital acceleration hardly affects the precipitation EOFs.

Figure 9 displays the temporal evolution of the Atlantic Meridional Overturning Circulation (AMOC) during both interglacials. During the PIG, the AMOC generally shows a decreasing trend, whereas an increasing trend is simulated for the LIG. Rather surprisingly, the long-term LIG AMOC trend is hardly affected by the acceleration.

Effects of orbital acceleration on interglacial climates

V. Varma et al.

Title Page

Abstract

Introduction

Conclusions

References

Tables

Figures



Back

Close

Full Screen / Esc

Printer-friendly Version

Interactive Discussion



stratified, the effect of orbital acceleration on surface winds and (monsoonal) rainfall is negligible (cf. Govin et al., 2014).

In summary, it can be stated that results from orbitally accelerated interglacial CGCM simulations are meaningful for many applications. Except for some high-latitude regions, in particular the Southern Ocean, the acceleration technique does neither hamper model intercomparison nor model-data comparison studies such as, e.g., Bakker et al. (2013, 2014) and Kwiatkowski et al. (2015), in which accelerated simulations have been employed.

5 Conclusions

Transient simulations from a fully coupled comprehensive climate model have been analysed to study the effects of orbital acceleration on the present and last interglacial climates. To this end, simulations were carried out both with and without orbital acceleration. Comparison of the results shows that, in most parts of the world, the simulation of long-term variations in interglacial surface climate is not significantly affected by the use of the acceleration technique (with an acceleration factor 10) and hence model-data comparison of surface variables is therefore not hampered. However, due to the long adjustment time of the deep ocean with its huge heat reservoir, major repercussions of the orbital forcing are obvious below the thermocline. As a result, acceleration-induced biases in sea-surface temperature evolution arise in regions where the surface climate has a direct connection to the deep ocean (upwelling of deep water in the Southern Ocean, deep convection regions at high latitudes). In these regions, the climate trajectory can be significantly biased by an inappropriate initialization of the transient simulation. It was further found that the temporal evolution of the southern westerlies could be affected by temperature biases in the Southern Ocean. As such, the acceleration technique may compromise transient climate simulations over large regions in the Southern Hemisphere, where special care has to be taken.

Effects of orbital acceleration on interglacial climates

V. Varma et al.

Title Page

Abstract

Introduction

Conclusions

References

Tables

Figures



Back

Close

Full Screen / Esc

Printer-friendly Version

Interactive Discussion



Effects of orbital acceleration on interglacial climates

V. Varma et al.

Title Page

Abstract

Introduction

Conclusions

References

Tables

Figures



Back

Close

Full Screen / Esc

Printer-friendly Version

Interactive Discussion



Acknowledgements. The CCSM3 simulations were performed on the SGI Altix supercomputer of the Norddeutscher Verbund für Hoch- und Höchstleistungsrechnen (HLRN). This work was funded through the DFG Priority Research Program INTERDYNAMIK and the European Union's Seventh Framework Programme (FP7/2007-2013) under grant agreement 243908, "Past4Future. Climate change – Learning from the past climate".

The article processing charges for this open-access publication were covered by the University of Bremen.

References

- Bakker, P., Stone, E. J., Charbit, S., Gröger, M., Krebs-Kanzow, U., Ritz, S. P., Varma, V., Khon, V., Lunt, D. J., Mikolajewicz, U., Prange, M., Renssen, H., Schneider, B., and Schulz, M.: Last interglacial temperature evolution – a model inter-comparison, *Clim. Past*, 9, 605–619, doi:10.5194/cp-9-605-2013, 2013.
- Bakker, P., Masson-Delmotte, V., Martrat, B., Charbit, S., Renssen, H., Gröger, M., Krebs-Kanzow, U., Lohman, G., Lunt, D. J., Pfeiffer, M., Phipps, S. J., Prange, M., Ritz, S. P., Schulz, M., Stenni, B., Stone, E. J., and Varma, V.: Temperature trends during the present and last interglacial periods – a multi-model-data comparison, *Quaternary Sci. Rev.*, 99, 224–243, doi:10.1016/j.quascirev.2014.06.031, 2014.
- Berger, A. L.: Long-term variations of daily insolation and Quaternary climatic changes, *J. Atmos. Sci.*, 35, 2362–2367, doi:10.1175/1520-0469(1978)035<2362:LTVODI>2.0.CO;2, 1978.
- Braconnot, P., Otto-Bliesner, B., Harrison, S., Joussaume, S., Peterchmitt, J.-Y., Abe-Ouchi, A., Crucifix, M., Driesschaert, E., Fichet, Th., Hewitt, C. D., Kageyama, M., Kitoh, A., Laîné, A., Loutre, M.-F., Marti, O., Merkel, U., Ramstein, G., Valdes, P., Weber, S. L., Yu, Y., and Zhao, Y.: Results of PMIP2 coupled simulations of the Mid-Holocene and Last Glacial Maximum – Part 1: experiments and large-scale features, *Clim. Past*, 3, 261–277, doi:10.5194/cp-3-261-2007, 2007.
- Claussen, M., Mysak, L. A., Weaver, A. J., Crucifix, M., Fichet, T., Loutre, M.-F., Weber, S. L., Alcamo, J., Alexeev, V. A., Berger, A., Calov, R., Ganopolski, A., Goosse, H., Lohmann, G., Lunkeit, F., Mokhov, I. I., Petoukhov, V., Stone, P., and Wang, Z.: Earth system models of

Effects of orbital acceleration on interglacial climates

V. Varma et al.

Title Page

Abstract

Introduction

Conclusions

References

Tables

Figures



Back

Close

Full Screen / Esc

Printer-friendly Version

Interactive Discussion



intermediate complexity: closing the gap in the spectrum of climate system models, *Clim. Dynam.*, 18, 579–586, 2002.

Collins, W. D., Bitz, C. M., Blackmon, M. L., Bonan, G. B., Bretherton, C. S., Carton, J. A., Chang, P., Doney, S. C., Hack, J. J., Henderson, T. B., Kiehl, J. T., Large, W. G., McKenna, D. S., Santer, B. D., and Smith, R. D.: The Community Climate System Model Version 3 (CCSM3), *J. Climate*, 19, 2122–2143, doi:10.1175/JCLI3761.1, 2006.

Kwiatkowski, C., Prange, M., Varma, V., Steinke, S., Hebbeln, D., and Mohtadi, M.: Holocene variations of thermocline conditions in the eastern tropical Indian Ocean, *Quaternary Sci. Rev.*, 114, 33–42, doi:10.1016/j.quascirev.2015.01.028, 2015.

Liu, Z., Zhu, J., Rosenthal, Y., Zhang, X., Otto-Bliesner, B. L., Timmermann, A., Smith, R. S., Lohmann, G., Zheng, W., and Elison Timm, O.: The Holocene temperature conundrum, *P. Natl. Acad. Sci. USA*, 111, E3501–E3505, doi:10.1073/pnas.1407229111, 2014.

Lorenz, S. J. and Lohmann, G.: Acceleration technique for Milankovitch type forcing in a coupled atmosphere–ocean circulation model: method and application for the Holocene, *Clim. Dynam.*, 23, 727–743, 2004.

Loulergue, L., Schilt, A., Spahni, R., Masson-Delmotte, V., Blunier, T., Lemieux, B., Barnola, J.-M., Raynaud, D., Stocker, T. F., and Chappellaz, J.: Orbital and millennial-scale features of atmospheric CH₄ over the past 800,000 years, *Nature*, 453, 383–386, doi:10.1038/nature06950, 2008.

Lunt, D. J., Williamson, M. S., Valdes, P. J., Lenton, T. M., and Marsh, R.: Comparing transient, accelerated, and equilibrium simulations of the last 30 000 years with the GENIE-1 model, *Clim. Past*, 2, 221–235, doi:10.5194/cp-2-221-2006, 2006.

Lunt, D. J., Abe-Ouchi, A., Bakker, P., Berger, A., Braconnot, P., Charbit, S., Fischer, N., Herold, N., Jungclaus, J. H., Khon, V. C., Krebs-Kanzow, U., Langebroek, P. M., Lohmann, G., Nisancioglu, K. H., Otto-Bliesner, B. L., Park, W., Pfeiffer, M., Phipps, S. J., Prange, M., Rachmayani, R., Renssen, H., Rosenbloom, N., Schneider, B., Stone, E. J., Takahashi, K., Wei, W., Yin, Q., and Zhang, Z. S.: A multi-model assessment of last interglacial temperatures, *Clim. Past*, 9, 699–717, doi:10.5194/cp-9-699-2013, 2013.

Lüthi, D., Le Floch, M., Bereiter, B., Blunier, T., Barnola, J.-M., Siegenthaler, U., Raynaud, D., Jouzel, J., Fischer, H., Kawamura, K., and Stocker, T. F.: High-resolution carbon dioxide concentration record 650,000–800,000 years before present, *Nature*, 453, 379–382, doi:10.1038/nature06949, 2008.

Effects of orbital acceleration on interglacial climates

V. Varma et al.

Title Page

Abstract

Introduction

Conclusions

References

Tables

Figures



Back

Close

Full Screen / Esc

Printer-friendly Version

Interactive Discussion



- Merkel, U., Prange, M., and Schulz, M.: ENSO variability and teleconnections during glacial climates, *Quaternary Sci. Rev.*, 29, 86–100, doi:10.1016/j.quascirev.2009.11.006, 2010.
- Milker, Y., Rachmayani, R., Weinkauf, M. F. G., Prange, M., Raitzsch, M., Schulz, M., and Kučera, M.: Global and regional sea surface temperature trends during Marine Isotope Stage 11, *Clim. Past*, 9, 2231–2252, doi:10.5194/cp-9-2231-2013, 2013.
- Otto-Bliesner, B. L., Russell, J. M., Clark, P. U., Liu, Z., Overpeck, J. T., Konecky, B., deMenocal, P., Nicholson, S. E., He, F., and Lu, Z.: Coherent changes of southeastern equatorial and northern African rainfall during the last deglaciation, *Science*, 346, 1223–1227, 2014.
- Smith, R. and Gregory, J.: The last glacial cycle: transient simulations with an AOGCM, *Clim. Dynam.*, 38, 1545–1559, doi:10.1007/s00382-011-1283-y, 2012.
- Spahni, R., Chappellaz, J., Stocker, T. F., Loulergue, L., Hausammann, G., Kawamura, K., Fluckiger, J., Schwander, J., Raynaud, D., Masson-Delmotte, V., and Jouzel, J.: Atmospheric methane and nitrous oxide of the late pleistocene from Antarctic ice cores, *Science*, 310, 1317–1321, 2005.
- Timm, O. and Timmermann, A.: Simulation of the last 21,000 years using accelerated transient boundary conditions, *J. Climate*, 20, 4377–4401, 2007.
- Varma, V., Prange, M., Merkel, U., Kleinen, T., Lohmann, G., Pfeiffer, M., Renssen, H., Wagner, A., Wagner, S., and Schulz, M.: Holocene evolution of the Southern Hemisphere westerly winds in transient simulations with global climate models, *Clim. Past*, 8, 391–402, doi:10.5194/cp-8-391-2012, 2012.
- Voigt, I., Chiessi, C. M., Prange, M., Mulitza, S., Groeneveld, J., Varma, V., and Henrich, R.: Holocene shifts of the southern westerlies across the South Atlantic, *Paleoceanography*, 30, 39–51, doi:10.1002/2014PA002677, 2015.
- Yeager, S. G., Shields, C. A., Larger, W. G., and Hack, J. J.: The low-resolution CCSM3, *J. Climate*, 19, 2545–2566, doi:10.1175/JCLI3744.1, 2006.

Effects of orbital acceleration on interglacial climates

V. Varma et al.

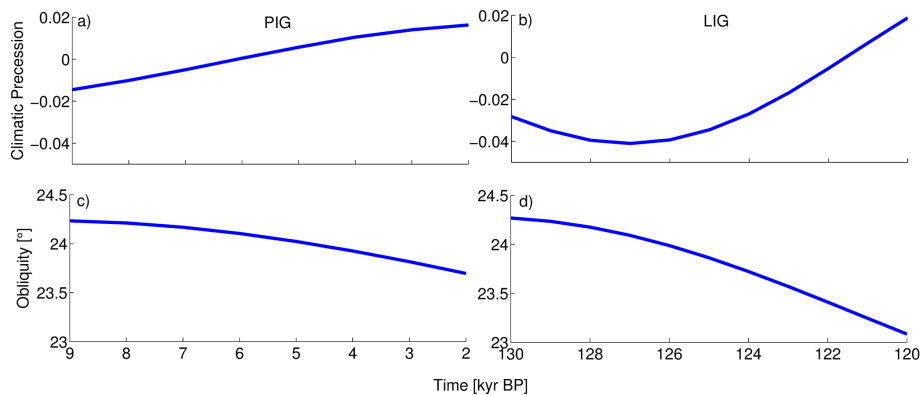


Figure 1. Orbital parameters in the transient experiments for the PIG (a, c) and the LIG (b, d) (Berger, 1978).

[Title Page](#)[Abstract](#)[Introduction](#)[Conclusions](#)[References](#)[Tables](#)[Figures](#)[Back](#)[Close](#)[Full Screen / Esc](#)[Printer-friendly Version](#)[Interactive Discussion](#)

Effects of orbital acceleration on interglacial climates

V. Varma et al.

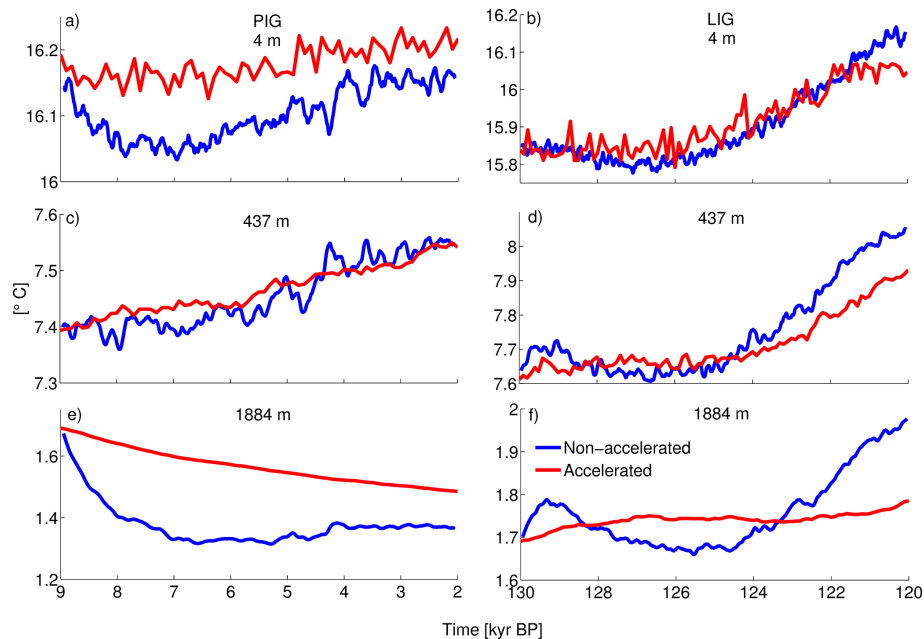


Figure 2. Evolution of global mean potential ocean temperature at various depths for the PIG (a, c, e) and the LIG (b, d, f). Blue lines represent the non-accelerated simulations and red lines represent the accelerated simulations. All plots were created using the decadal mean values (referring to model years). In addition, a 10-point running average was applied to the decadal mean values of the non-accelerated simulations.

Title Page

Abstract

Introduction

Conclusions

References

Tables

Figures



Back

Close

Full Screen / Esc

Printer-friendly Version

Interactive Discussion



Effects of orbital acceleration on interglacial climates

V. Varma et al.

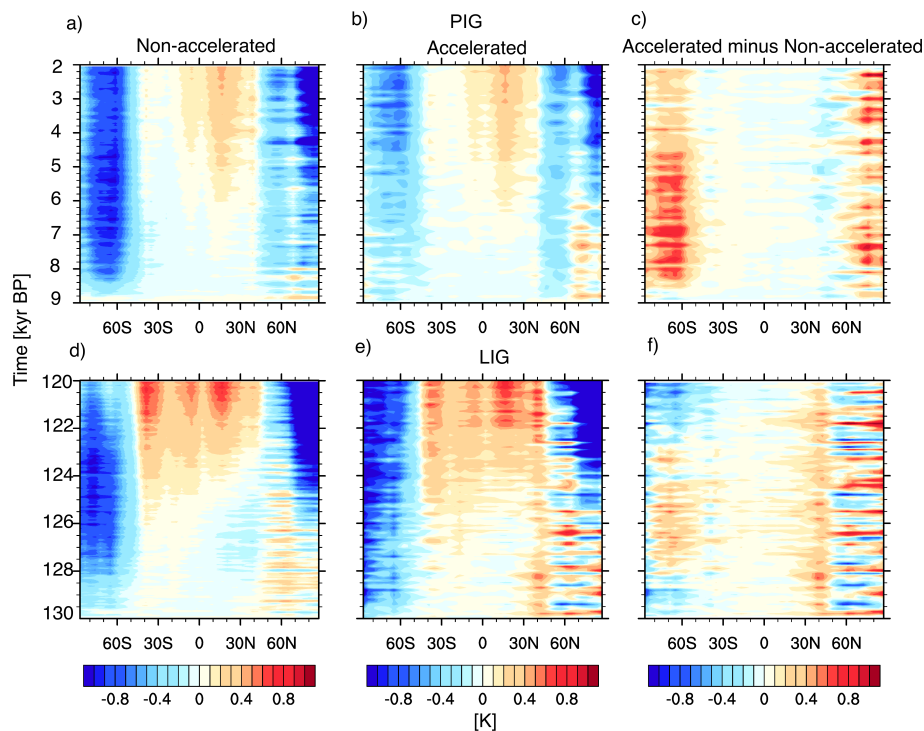


Figure 3. Evolution of zonally averaged surface temperature anomalies (including ocean and land) during the interglacials for both non-accelerated (**a, d**) and accelerated (**b, e**) simulations. Shown are anomalies relative to the 9 kyr BP (PIG) and 130 kyr BP (LIG) states. Differences in the temperature evolution between accelerated and non-accelerated simulations are also displayed (**c, f**). All plots were created using the decadal mean values (referring to model years). In addition, a 10-point running average was applied to the decadal mean values of the non-accelerated simulations.

Effects of orbital acceleration on interglacial climates

V. Varma et al.

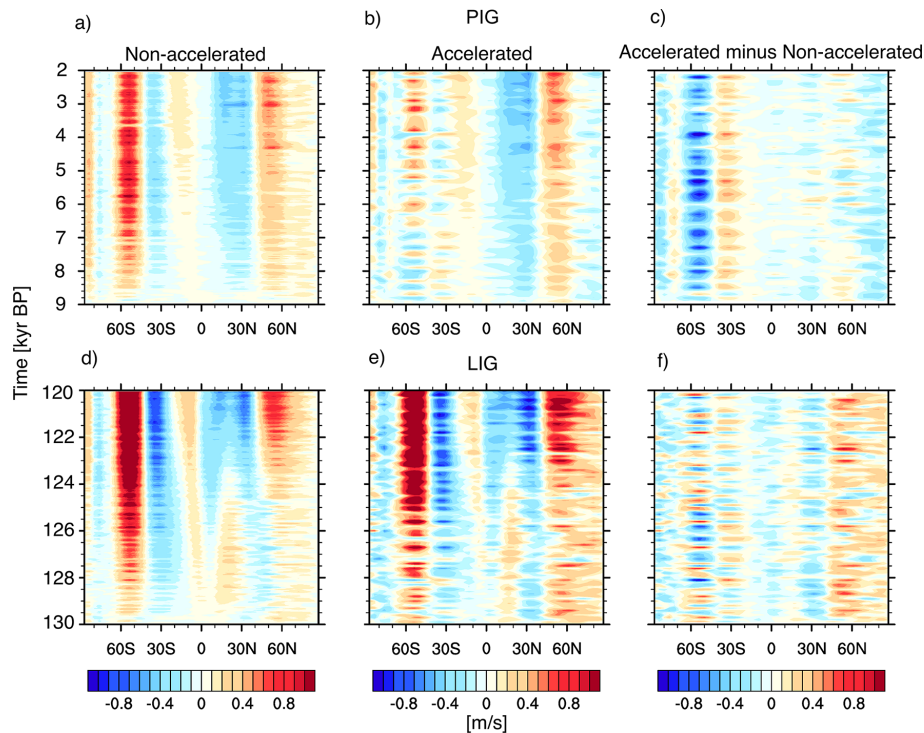


Figure 4. Same as Fig. 3 but for 850 hPa zonal wind.

Title Page

Abstract

Introduction

Conclusions

References

Tables

Figures



Back

Close

Full Screen / Esc

Printer-friendly Version

Interactive Discussion



Effects of orbital acceleration on interglacial climates

V. Varma et al.

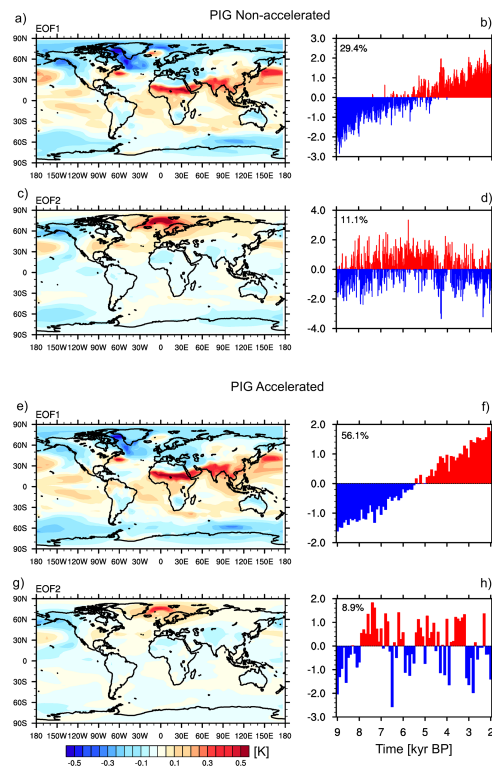


Figure 5. Leading two EOFs of annual-mean surface temperature calculated from the non-accelerated (a–d) and accelerated (e–h) PIG simulations. Explained variances of each EOF are specified in the principal component (time series) plots (b, d, f, h). All EOF analyses were performed on serial decadal mean values (referring to model years) from the transient simulations. Principal components are standardized and the EOF maps (a, c, e, g) were obtained by regressing the surface temperature data onto the corresponding standardized principal component time series.

Effects of orbital acceleration on interglacial climates

V. Varma et al.

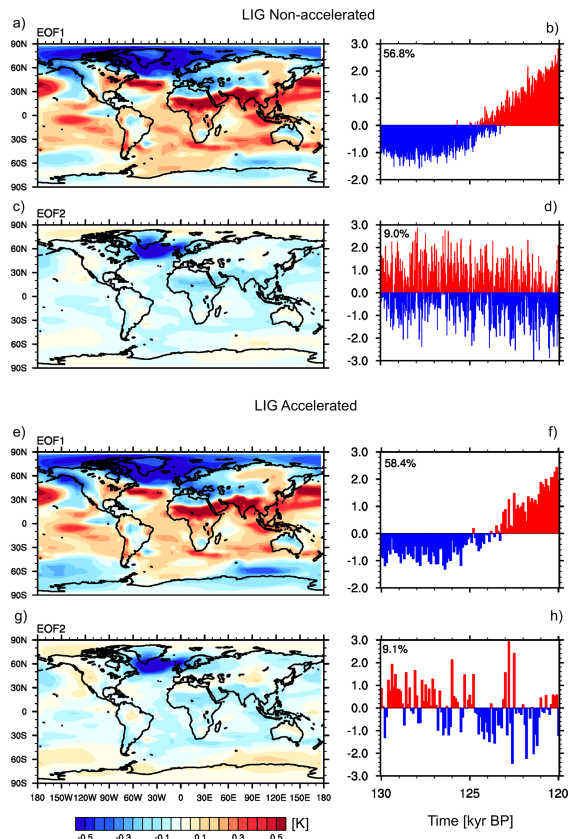


Figure 6. Same as Fig. 5 but for the LIG simulations.

[Title Page](#)

[Abstract](#) [Introduction](#)

[Conclusions](#) [References](#)

[Tables](#) [Figures](#)

[◀](#) [▶](#)

[◀](#) [▶](#)

[Back](#) [Close](#)

[Full Screen / Esc](#)

[Printer-friendly Version](#)

[Interactive Discussion](#)



Effects of orbital acceleration on interglacial climates

V. Varma et al.

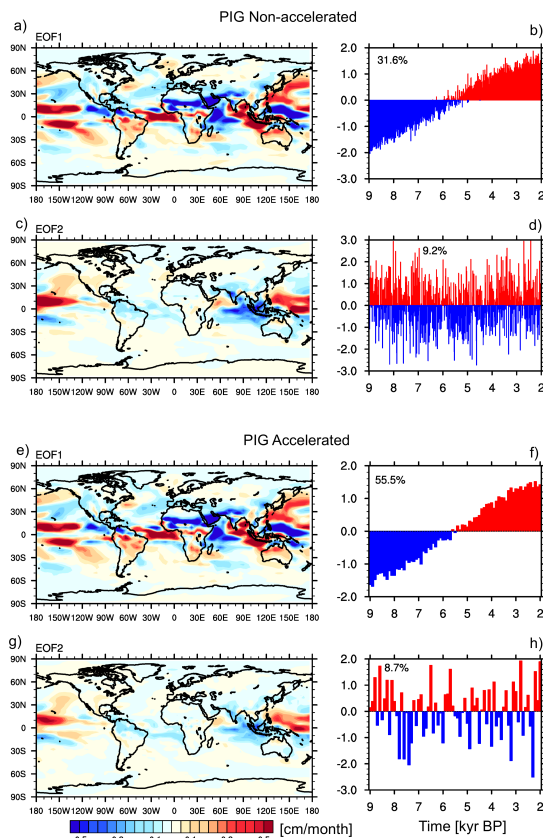


Figure 7. Same as Fig. 5 but for annual precipitation.

Effects of orbital acceleration on interglacial climates

V. Varma et al.

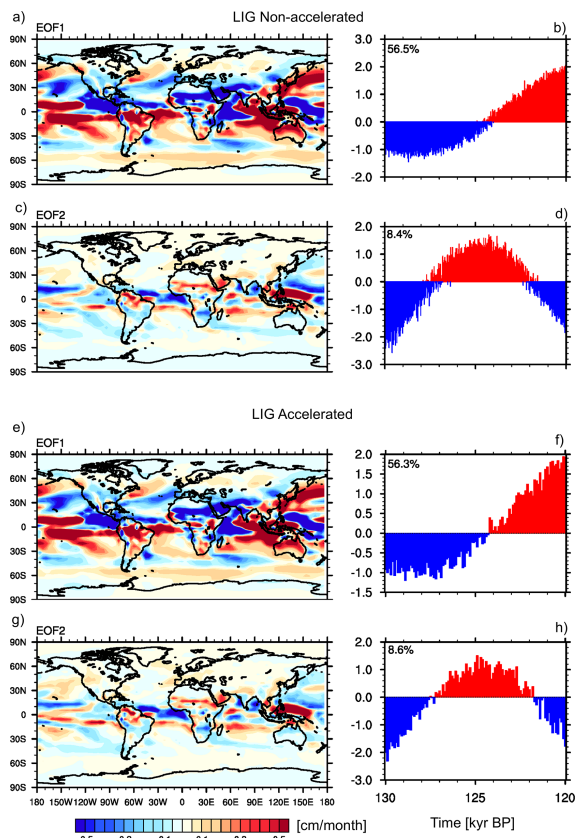


Figure 8. Same as Fig. 7 but for the LIG simulations.

Title Page

Abstract	Introduction
Conclusions	References
Tables	Figures

⏪ ⏩
◀ ▶
 Back Close

Full Screen / Esc

Printer-friendly Version

Interactive Discussion



Effects of orbital acceleration on interglacial climates

V. Varma et al.

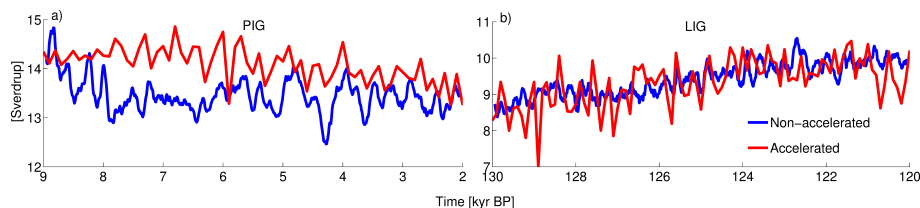


Figure 9. Temporal evolution of the Atlantic Meridional Overturning Circulation (given as the maximum of the North Atlantic overturning streamfunction) during both the interglacials for both non-accelerated (blue) and accelerated (red) simulations. All plots were created using the decadal mean values (referring to model years). In addition, a 10-point running average was applied to the decadal mean values of the non-accelerated simulations.

[Title Page](#)[Abstract](#)[Introduction](#)[Conclusions](#)[References](#)[Tables](#)[Figures](#)[⏪](#)[⏩](#)[◀](#)[▶](#)[Back](#)[Close](#)[Full Screen / Esc](#)[Printer-friendly Version](#)[Interactive Discussion](#)